



Probable two-layered permafrost formation, as a result of climatic evolution in mountainous environment of Storglaciären forefield, Tarfala, Northern Scandinavia

Wojciech DOBIŃSKI* and Michał GLAZER

University of Silesia, Faculty of Earth Sciences, ul. Będzińska 60, 41-200 Sosnowiec, Poland

* *corresponding author <wojciech.dobinski@us.edu.pl>*

Abstract: The analysis of climate changes in of the Tarfala valley and Kebnekaise Mts area, and changes within the range of the Scandinavian Glaciation shows that even in the warmest period of Holocene there were favourable environmental conditions for permafrost of the Pleistocene origin to be preserved in this area. The results of electrical resistivity surveys together with analysis of available publications indicate that two layers of permafrost can be distinguished in the Storglaciären forefield. The shallower, discontinuous, with thickness *ca.* 2–6 meters is connected to the current climate. The second, deeper located layer of permafrost, separated with talik, is older. Its thickness can reach dozens of metres and is probably the result of permafrost formation during Pleistocene. The occurrence of two-layered permafrost in the Tarfala valley in Kebnekaise area shows the evolution of mountain permafrost may be seen as analogous to that in Western Siberia. This means that the effect of climate changes gives a similar effect in permafrost formation and evolution in both altitudinal and latitudinal extent. The occurrence of two-layered permafrost in Scandes and Western Siberia plain indicates possible analogy in climatic evolution, and gives opportunity to understand them in uniform way.

Key words: Scandinavia, permafrost evolution, two-layered permafrost, ERT.

Introduction

Permafrost studies are currently concentrated in two parallel directions: the first is the study of Arctic permafrost, the second is related to mountain permafrost research. Both are dominated by contemporary, active permafrost, *i.e.* permafrost which reacts to modern climate change (Dobiński 2017). In this way, the attention paid to the role of the fossil permafrost, which has a dominant role on the Earth lithosphere, seems to decrease slightly. In general, permafrost is predominantly

a relict of the Pleistocene period. One of important aspects of its research in high mountain environments, which is not often taken in to consideration at present, is the evolution of permafrost in time and space, which can be analogous to the Arctic permafrost. The purpose of this paper is to present the results of permafrost studies performed on the forefield of Storglaciären in the Kebnekaise area, northern Sweden, which indicate the possibility of permafrost existence in two subsequent layers: younger, contemporary permafrost and older one located underneath. Because permafrost is present in the two-layer form also in Western Siberia, the secondary purpose of the work is to try to find similarity between mountainous and Arctic permafrost. The main hypothesis assumes that the evolution of permafrost in mountains of northern Scandinavia is analogous to the evolution of permafrost in Western Siberia, so there is a possibility and perhaps also a need for a common perception of both of them. The empirical research is based on the results of electrical resistivity tomography surveys performed in the area relatively well known for the presence of permafrost. Fieldwork was focused therefore on greater research depth than was achieved in previous works made in this area by other authors (Dobiński *et al.* 2017). The analysis and discussion of the results is based also on the information on postglacial climate evolution, the thermal characteristics and changes of Pleistocene glaciation, and the possibility of similar cases in other mountainous regions.

Fieldwork was concentrated on identification of vertical permafrost extent and the results obtained show the geophysical structure of permafrost on the glacier forefield between its current margin, and position left by the glacier *ca.* 60 years ago or earlier. Research results along with the literature review on the specificity of the mountain permafrost occurrence in other locations, and especially the permafrost of the Western Siberia, allow to present a new hypothesis concerning the permafrost evolution, which gives possibility for uniform treatment of permafrost in the both: altitudinal and latitudinal periglacial environments in time and space, particularly when the last glaciation was finished. The final result of the work presents a theoretical model of the mountain permafrost, which can be used for modification of boundary conditions in computer modelling to better approach its development and evolution. Determination of the active layer depth in the glacier forefield as well as the glacier – permafrost relation is described in more details by authors in another paper (Dobiński *et al.* 2017).

Study area

The Tarfala Valley (Fig. 1) and its surroundings are located in the highest parts of the northern Scandinavian Mountains near Kebnekaise Mts, on the eastern part of the Kebnekaise massif (2117 m a.s.l.). The Storglaciären is situated at 67°54'09.1N, 18°35'18.3E. The mean annual air temperature at the Tarfala Research Station

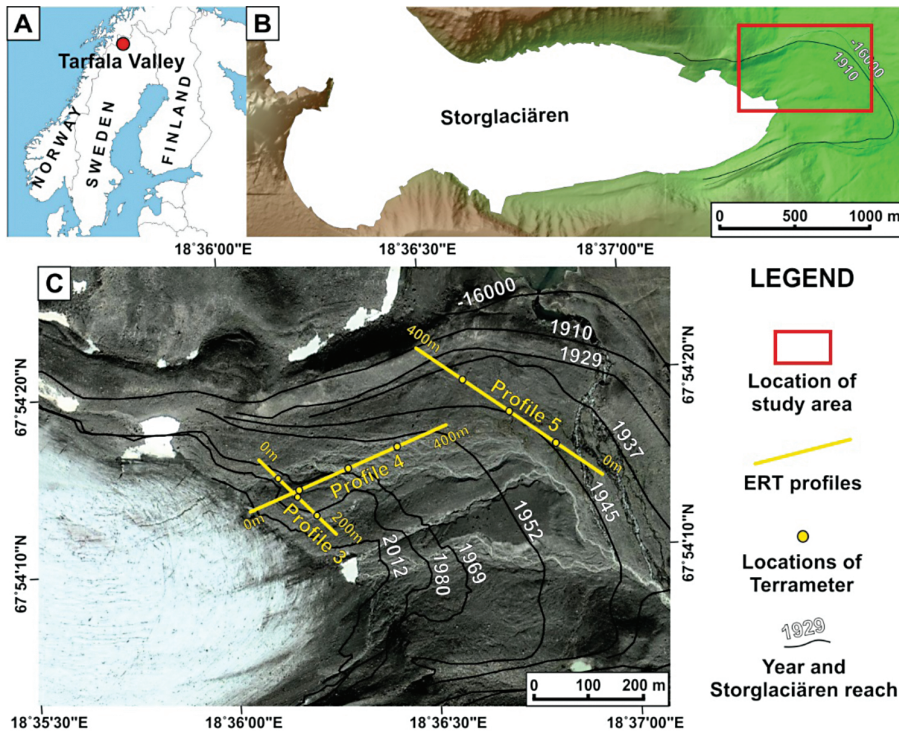


Fig. 1. Maps of the study area: (A) Simplified map presenting position of Tarfala Valley, (B) Location of the research area on the Storglaciären forefield, (C) Location of ERT profiles and ranges of Storglaciären in selected years (DEM and ranges of glacier by courtesy of Tarfala Research Station, Satellite image by ©2015 Google maps).

nearby (1135 m a.s.l.) is -3.5°C , over the period 1965–2011 (Jonsell *et al.* 2013) (Fig. 2). Mean annual precipitation is *ca.* 2000 mm (Dahlke *et al.* 2012). The first approximation for estimating the potential of ground freezing and thawing is the relationship of freezing (FI) and thawing (TI) indexes (Harris 1981, 1982). Data from 1965–2011 shows a warming trend for both data series. However, the warming trend of TI is smaller than the warming trend of FI. This means that the potential of ground freezing decreases more intensely than grows the potential of thawing of the ground in the same time (Fig. 3). The summer temperature lapse rate is $0.7^{\circ}\text{C}/100\text{ m}$, whereas in the winter temperature lapse rate is inverse with $-0.6^{\circ}\text{C}/100\text{ m}$ due to lower winter temperatures in the Ladstjovagge valley than in Tarfala. Dwarf shrubs, mainly *Salix* appear up to 1000 m a.s.l. and the birch forest reaches up to 700–750 m a.s.l. (Fuchs 2013).

The Storglaciären and its forefield is entirely located within the Seve Nappe Complex of the Scandinavian Caledonides. Its main tectonostratigraphy units are Tarfala Amphibolite, the Storglaciären Mylonite Gneiss, Kebne Amphibolite, and

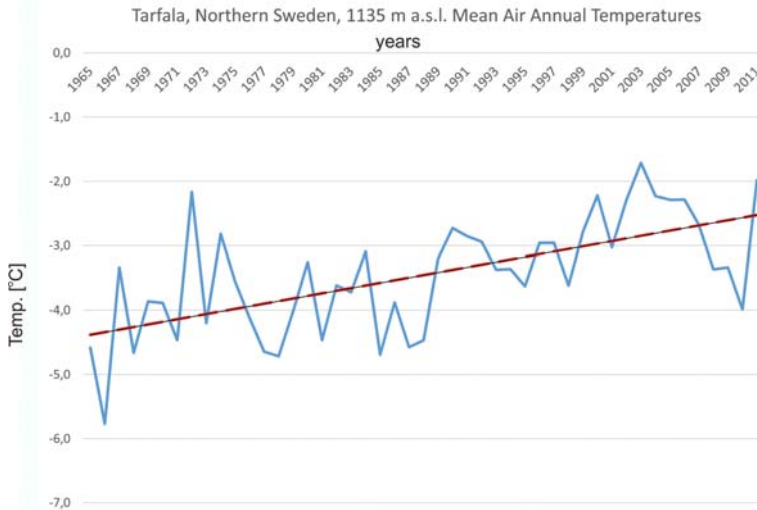


Fig. 2. Changes of mean annual air temperatures at Tarfala Research Stations (Tarfala Research Station) in years 1965–2011. Data courtesy of Tarfala Research Station.

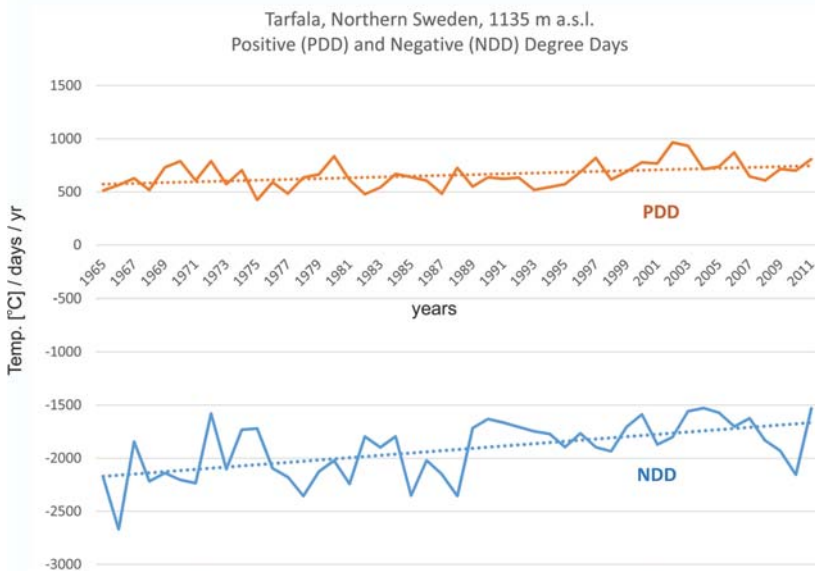


Fig. 3. Freezing and thawing indices at Tarfala Research Station showing thermal potential for ground freezing and thawing balance. Data courtesy of Tarfala Research Station.

the Kebne Dyke Complex (Baird 2005). Beneath this complex lies the middle allochthon – The Jåkk Mylonite Gneiss. This nappe succession dip 20–40° to the northwest. Its deepest units may be observed in Tarfalayak, downstream from the hydrology station. From there the autochthonous base formed as Precambrian granitoids emerge (Andréasson and Gee 1989; Baird 2005). Most Storglaciären forefield and valley floor is covered by the glacial sediment deposits. The Kebnekaise geomorphology is a result of long-lasting glaciation, which creates a high-mountain environment with all characteristic components, reworked by periglacial activity during the postglacial period.

The impact of highly diverse, mountainous environment has fundamental consequence for the distribution of mountain permafrost. It makes its detection more difficult, *e.g.* through the lack of favourable conditions for the development of geomorphic forms indicative for permafrost. Continentality of climate is another point of uncertainty. Both southern and northern Norway mountain ranges are influenced by maritime climatic conditions in west and more continental climate type in the east (see Table 1).

Table 1

West – East continentality increase on the distance of *ca.* 100 km in Northern Sweden (compiled after Ridfeldt and Boelhouwers 2006; Jonasson 1991).

MAAT – Mean Annual Air Temperature

Station	Location	Elevation (m a.s.l.)	MAAT (°C)	Precipitation (mm)
Riksgränsen	68°25'N 18°07'E	508	-1.5	940
Bjorkliden	68°24'N 18°41'E	360	no data	848
Abisko	68°21'N 18°48'E	388	-0.8	304
Torneträsk	68°13'N 20°28'E	393	-1.0	428

Materials and Methods

Glaciation and conditions favourable for subglacial permafrost development. — Climatic evolution of Northern Scandinavia and accompanying glaciation is the precondition which should be taken into consideration first. The latest review of the Fennoscandian Ice Sheet models has been recently published (Schmidt *et al.* 2014). This study presents analysis of possible ice-sheet configurations and glacial isostatic adjustment. Three modern models, *i.e.*

UMISM (2010), ICE-5G (2004) and AMU (2010) were selected in this work. We used the result presented in this paper to describe the volume, areal extent, mean and maximum thickness of the Scandinavian Ice Sheet during last glaciation. For the purposes of this paper, two basic facts are of essence: (1) glaciation lasted in the Scandinavia uninterrupted from *ca.* 69 kyr B.P. to *ca.* 10 kyr B.P.; and (2) the mean thickness of ice in that period oscillated from *ca.* 500 to 1500 m at the end, *i.e.* in the Last Glacial Maximum, while the maximum thickness was from *ca.* 800 to nearly 4000 m. In the Kebnekaise area, the thickness of ice – depending on time and model type – ranges from *ca.* 1800 to *ca.* 2800 m during this period (see also Siegert *et al.* 2001). In the northern part of the Scandinavian Mountains, ice-sheet retreated in *ca.* 8000 yr B.P., and as evidenced by glaciological modelling and geomorphological studies, it was built of ‘cold’ ice and was frozen to the bedrock during the entire glaciation period *ca.* 60 kya (Kleman and Glasser 2007; Kleman *et al.* 2008; Lilleøren *et al.* 2012; Schmidt *et al.* 2014). The ice sheet was surely more domed as its movement capacity was limited and based mainly on plastic deformation, no basal sliding (Kleman and Glasser 2007; Kleman *et al.* 2008). In consequence also block fields and patterned ground on mountains and plateaux survived glaciation beneath cold ice (Winkler *et al.* 2016). The temperature under the frozen ice-sheet must have been significantly lower than the pressure melting point (PMP). Pressure at the base of 2000 m thick ice-sheet is *ca.* 17.6 MPa, and it is enough to lower the melting point to -1.27°C . (Benn and Evans 1998). Such a thermal state must have caused permafrost aggradation in it. And even if the temperature on the ice/ground interface was not very low, the lack of seasonal thawing in summer, which under periglacial conditions, leading to seasonal reversal of thermal flow direction in the ground, together with the permanence of the frozen ice sheet can cause frost penetration relatively deep. Freezing of the ground under the “cold ice” could have been relatively slow, however, but lasting long enough allowing for development of permafrost layer of significant thickness. Heat penetration depends on different conductivity coefficient in frozen and thawed ground, where frozen ground typically has higher thermal conductivities than thawed ground. This implies progressively colder temperatures down, and makes it possible to maintain permafrost also when the mean annual ground surface temperature (MAGST) is close to or above 0°C (Lilleøren *et al.* 2012). The issue of sub-glacial modelling of permafrost aggradation/degradation is not covered adequately in the literature. Actually it is difficult to find the estimations of frost penetration rate or calculations of the thickness of sub-glacial permafrost. On the other hand we have to take into consideration that in the postglacial period the mean annual air temperature (MAAT) value in the highest part of the Scandinavian Mountains was never above 0°C , so it has to be assumed that during the entire Holocene there were no climatic conditions which made possible even to just start the permafrost degradation in the highest parts of

Tarfala/Kebnekaise area. Periodical change in active layer depth and other shallow processes (see chapter 4.1) were, however, possible. There was also no sufficiently long period of time with higher temperature, which would allow for full degradation of mountain permafrost developed in the glaciation period and right after ice-sheet retreat. The paper that shows how slow this process is in much warmer regions was published by Šafanda *et al.* (2004).

It is worth to notice, that specific conditions for the aggradation of permafrost in the ground appear when glaciation retreats. In the sufficiently high mountains, the periglacial climate conditions favourable for permafrost aggradation (*i.e.* MAAT $<0^{\circ}\text{C}$) occur both: above and below the glaciated area. As a result, retreat of glaciation does not force permafrost to degrade, it may even result in the permafrost aggradation on a glacier forefield. Such process may occur in Scandinavian Mountains as well (Kneisel 1999).

Also, the rate of degradation of Pleistocene permafrost in Central European Lowlands (CEL) is not sufficiently studied and relict permafrost may occur in places that surprise scientists. In northern part of CEL in Poland, actually with MAAT *ca.* 7°C within Suwałki Anorthosite Massif near Udryn, Suwałki area, occurrence of *ca.* 110–150 m thick permafrost at the depth below 357 m with extend over 50 km² and permafrost base located at *ca.* 470–500 m was proved based on a direct borehole temperature measurements and thermal modelling. (Szewczyk and Nawrocki 2011; Szewczyk 2017). This finding essentially changes the way of thinking at the occurrence of fossil permafrost, including the mountainous areas as well. Analogically, basing exclusively on this assumption, the existence of fossil permafrost in the Scandinavian Mountains can not be excluded.

The identification of climate changes that occurred in the last *ca.* 10 000 years in the northern Scandinavia is based on the analysis of a series of sediment cores obtained from proglacial lakes, ¹⁴C datings of moraines, lichenometry datings and ¹⁴C datings defining the variability of forest border position. A substantial part of northern Lapland was deglaciated before 9000–8500 ¹⁴C yr B.P. A minimum date reported is 8480 ± 155 ¹⁴C yr B.P. (Karlén 1979). The deglaciation of the areas located at a higher altitude must have occurred later. In his earlier work, Karlén (1976) describes the climate changes in the Holocene in more detail. The upper tree-line during the Holocene Thermal Maximum (HTM) was probably only 150–190 m higher than currently (Kullman and Kjälgren 2006; Lilleøren *et al.* 2012). Presently dwarf shrubs, mainly *Salix*, appear up to 1000 m a.s.l. and the birch forest reaches up to 700–750 m a.s.l. (Fuchs 2013). During the entire Holocene the area of the Tarfala valley and its surroundings was always at most at the forest border and the Storglaciären together with its forefield never witnessed the presence of trees in that period. This indirect information indicate the favourable conditions for permafrost existence and evolution which take the place during entire period since the end of Pleistocene glaciation of that valley.

Previous permafrost studies in Scandinavia. — The information on the occurrence of mountain permafrost in Scandinavia up to about mid-1980s was scarce. The first reports come from the beginning of the 20th century; the researchers of that time, *i.e.* A. Hamberg, and B. Högbom (King 1986), suggested the widespread occurrence of that phenomenon, linked mainly with palsa bogs and peat bogs (Jeckel 1988; King 1986; Seppälä 1982; Åkerman and Malmstrom 1986) and specific land forms – ice-cored moraines in the Scandinavian Mts (Østrem 1964). The study by Ekman (1957) describes the drilling performed at 1220 m in the mountains, near Abisko, and the discovery of *ca.* 70 m thick permafrost. One of the first synthetic studies on the permafrost occurrence of in northern Sweden is a paper by Rapp (1982), where he presents a 1:250 000 geomorphological map based on an earlier study by Melander (1977). It shows geomorphological features (palsa bogs) which are indicative for the permafrost occurrence and can be found at the height below 600 m a.s.l., where the mean annual temperature is close or below -1°C . Palsas are related to the occurrence of the sporadic (island) permafrost zone in Fennoscandia.

In general, the lower limit of mountain permafrost in Scandinavia decreases from the western coast towards the more continental conditions in north-eastern Norway and Sweden, but the lower altitudinal limit of discontinuous and sporadic permafrost is not known precisely. Between the mountains in Troms and Finnmark in northern Norway, lower permafrost limit is located between 700–1200 m a.s.l. In the interior of Finnmarksvidda, the transect shows sporadic permafrost down to elevations of 400 m. (Gisnås *et al.* 2013). Similar values are presented by other authors. In Finnmark, the lower permafrost limit is expected at *ca.* 400–500 m a.s.l., discontinuous permafrost may exist as low as at 550 m a.s.l. in the interior part of the northern Scandinavian mountains, and above 990 m a.s.l. in the coastal mountains. In northernmost Norway, sporadic permafrost can exist close to sea level in palsas and peat plateaus (Ridefelt *et al.* 2008; Christiansen *et al.* 2010). In the area of Abisko in the Storflaket peat bog (*ca.* 400 m a.s.l.), geophysical studies on the permafrost occurrence were also conducted by Dobiński (2010, 2011b). The electrical resistivity tomography and refraction seismic study results indicate that the thickness of permafrost may be higher than assumed before, and reaches 30 m below the active layer. Seven new boreholes made in this area will give new insight in permafrost distribution in this area (Johansson *et al.* 2011). Glacier–permafrost relationship was also studied in Tarfala area on the forefield of Storglaciären (Kneisel 1999, 2003; Dobiński *et al.* 2011, 2017). Bearing in mind the definition of mountain permafrost connected with altitude 500 m a.s.l. (Gorbunov 1988), it might be observed an overlap of mountain and arctic permafrost in that region (Dobiński 2011b; Lilleøren *et al.* 2012).

Holocene permafrost evolution. — Post-glacial warming towards the Holocene Thermal Maximum (HTM) occurred more rapid in southern Norway than in the north, but the latest glacier advances of the Little Ice Age (LIA) took place in coastal environments simultaneously in northern and southern Norway around 1910s. LIA was the coldest time period since the Weichselian deglaciation making possible the deepest permafrost penetration into the ground. During the HTM all sites even at the highest altitudes underwent thaw and talik formation. Continuous permafrost conditions were possible before and after this period. Permafrost modelling based on data from uppermost borehole location in southern Norway, shows temperatures below 0°C through all parts of Holocene (Lilleøren *et al.* 2012). Therefore it is obvious that in the highest areas permafrost survived this period, and has persisted during all the Holocene and speculatively also during the Pleistocene under cold basal conditions of the ice-sheet. The areas of Holocene permafrost age are situated in all the highest mountain areas of southern Norway, such as Jotunheimen, Dovrefjell, and Rondane (Lilleøren *et al.* 2012). Analogically in northern Scandinavia its existence can not be excluded especially in Kebnekaise area.

Lilleøren *et al.* (2012) proposing new altitudinal zonation of permafrost during its Holocene evolution for the borehole sites in Norway. The uppermost two zones are situated above 1400 m a.s.l. in northern Norway and represent areas with extensive permafrost occurrence throughout the Holocene. Within the lower of these two zones permafrost might have survived the HTM below taliks. In northern Norway during the LIA most of Finnmarksvidda, plateau with elevations between 300 and 500 m a.s.l., was probably underlain by permafrost. The altitudinal boundary of no permafrost during Holocene is at least lower than these elevations in Finnmark, but permafrost could have been present down to sea level in favourable areas. In the coastal areas of Troms county, permafrost probably never occurred at elevations lower than 500 m a.s.l. while this boundary reach *ca.* 400 m a.s.l. in inner parts of Troms (Lilleøren *et al.* 2012).

The most bold estimations shows that the area subject to permafrost in Scandinavian Mts may reach *ca.* 100 000 km². It is more than the total of all such areas in other European mountains (except for Spitsbergen) (Gorbunov 2003). Contemporary modelling gives more precise results. For the period 1961–1990 it shows that total permafrost area in Norway encompass 10.0–10.8% of its entire area, compared to 6.1–6.4% for the period 1981–2010 (Gisnås *et al.* 2013). It means, that in the second case total permafrost area occupying between 19 100 and 20 300 km². In the subsequent papers (Gisnås *et al.* 2016) authors claims that, in total 25 400 km² (7.8%) of the Norwegian mainland is underlain by permafrost in an equilibrium with the climate over the 30-year period 1981–2010. About 70% of the modelled permafrost is situated within open, non-vegetated areas above the treeline.

During the LIA, the total area of mainland Norway underlain by permafrost was between 13.6 and 14.3% of and glacierised area is not considered in these values by the author (Gisnås *et al.* 2013). In this case, area encompassed by permafrost is estimated between *ca.* 44 000 and 46 400 km². In southern Norway, the southernmost location of continuous mountain permafrost is in the mountain massif of Gaustatoppen at 59°80' N, with continuous permafrost above 1700 m a.s.l. and discontinuous permafrost down to 1200 m a.s.l. The sporadic mountain permafrost extends around 200 m further down both in the western and eastern parts (Gisnås *et al.* 2016).

The vertical extent of permafrost in Scandinavia is less known than its horizontal range. Its thickness increases as the zones change from sporadic to continuous. Measurements carried out in 100 m deep drillhole in Tarfalaryggen and second 129 m deep in Juvvashoe shows that the permafrost in the southern part of the Scandinavian Mts extends deeper than in the north. Extrapolation of temperature at Juvvashoe (61°40'32"N, 8°22'04"E, 1894 m a.s.l.) indicate the permafrost thickness reach *ca.* 380 m (Isaksen *et al.* 2001). However, these are not direct data, they do not include the highest mountains environments. Gorbunov (2003) estimates, that the maximum thickness of permafrost under the highest Scandinavian peak (Galdhøpiggen, 61°38'07"N, 8°18'47"E, 2443 m a.s.l.) reaches 600 m, which means that its age may be at least several dozen thousand years.

Permafrost prospecting on Tarfala area and the Storglaciären forefield.

— The first electrical resistivity studies conducted in the Storglaciären forefield indicate frozen ground at the depth of *ca.* 4.6 m (Østrem 1964). Later on, more advanced geophysical studies with the electrical resistivity, seismic and BTS methods were conducted in Tarfala by King (1984). The electrical resistivity studies marked as G4 and G5 and the measurement of ground temperature in the Storglaciären forefield were also carried out by King (1984). The results indicate the presence of “high-resistivity permafrost” overlaying the layer of “low-resistivity permafrost” *ca.* 30–40 m thick. The measurements were made at the heights *ca.* 1040 and 1120 m a.s.l. The thickness of the active layer in this area is estimated to be 2–4 m and its resistivity—9000 Ωm. The permafrost found below has resistivity of about 100 times higher. The author does not exclude the presence of ice lenses in the ground. He also provides the value of resistivity for glacial ice, *i.e.* 40x10⁶ Ωm. The value of resistivity for ice-cored moraine was evaluated to be 30x10⁶ Ωm. According to this author, the forefield of Storglaciären has high-resistivity permafrost, which lies above the permafrost of lower resistivity (King 1984, p. 51). The author observes that there is relic permafrost as well. It is evident in the G3 sounding, performed on a slope of the Tarfala valley, near the Tarfalasjön lake, at the height of *ca.* 1250 m a.s.l.

King was succeeded by Kneisel (1999), who continued permafrost studies in the Storglaciären forefield and broadened their context by including glacier-

permafrost relation in their scope. Only in the central part of the forefield, the BTS measurements and Electroresistivity Tomography (ERT) soundings showed the presence of permafrost. Kneisel (1999, 2003), show that in the central part of the Storglaciären forefield permafrost is discontinuous. At nearby located Tarfalaryggen ridge (67°55'09"N, 1540 m a.s.l.), permafrost thickness is estimated to be *ca.* 350 m thick (Isaksen *et al.* 2001; Harris *et al.* 2001). In borehole situated at this place the geothermal gradient is small and negative in the upper 40–45 m. It changes from $-0.015^{\circ}\text{C m}^{-1}$ at 25 m to $0.010\text{--}0.011^{\circ}\text{C m}^{-1}$ at 95 m. Large-scale topographic influence may explain this specificity since adjacent valley is significantly deeper than the location of the boreholes. Undisturbed temperature field is located probably at least five to ten times deeper than drillhole (Christiansen *et al.* 2010). In the years 2003–2010 significant decrease in MAAT temperature from -1.7°C to -4.0°C was registered at Tarfala Station, which is also clearly marked in the recorded ground temperature at Tarfalaryggen drill site, at depth of 20 m in the years 2009–2011 and probably in the following years. Relatively deep heat transfer is possible due to very thin winter snow cover (<0.3 m) and relatively high thermal conductivity of the amphibolites from which the massif is built (Jonsell *et al.* 2013). Tarfalaryggen drill-hole is made on the altitude 1540 m a.s.l. *i.e.* 405 m higher than Tarfala Station. MAAT must be there *ca.* 2.5°C lower than in the valley and is close to -6°C . It gives there favorable conditions for continuous permafrost existence.

A new interesting input in permafrost understanding in the Tarfala area is shown by the results of the logistic regression, which was performed by Fuchs (2013) on the BTS values from King (1984), Marklund (2011), and those collected himself. The zonal borders of continuous permafrost with probability >0.9 are at 1422 m a.s.l., 1345 m a.s.l., and 1561 m a.s.l. according to King (1984), Marklund (2011) and Fuchs (2013), respectively. The occurrence of discontinuous permafrost with probability >0.5 is at 1212 m a.s.l. by King (1984), 1205 m a.s.l. by Marklund (2011) and 1219 m a.s.l. by Fuchs (2013). The lower border of sporadic permafrost is indicated at 1002 m a.s.l. by King (1984), 1064 m a.s.l. by Marklund (2011) and 875 m a.s.l. by Fuchs (2013).

In the area of the Storglaciären and its forefield, the research on glacier – permafrost relationship, were also performed, which is one of the most important interdisciplinary issues concerning the cryosphere (Dobiński 2012; Dobiński *et al.* 2017).

Research method. — Electroresistivity tomography (ERT) is frequently applied method for fast and low cost investigation of underground structure in non-invasive manner. Its basics are well described in literature (Dahlin 2001; Schrott and Sass 2008; Reynolds 2011; Loke *et al.* 2013). Because of the significant rise of electrical resistivity of the water during phase transition from

liquid to solid state, this method has become very popular choice for scientist that study permafrost occurrence and its spatial structure (Yoshikawa *et al.* 2006; Kneisel and Hauck 2008; Kneisel *et al.* 2008; Hilbich *et al.* 2009; Hauck 2013; You *et al.* 2013; Kasprzak 2015). During acquisition of the data, ABEM Terrameter LS has been used. On profile 3 the minimum electrode spacing has been set to 2.5 m while on profiles 4 and 5 it was 5 m. Measurements has been performed in August 2014. For increasing the information obtained on selected profiles, beyond Schlumberger array, additional measurements were carried out with utilization of dipole-dipol and Wenner protocols. Different arrays in ERT are characterized by different sensitivity for vertical and horizontal structures and by the strength of signal (Loke 2014). The profile 3 is exception from that. Due to the change of weather conditions, acquisition data from dipol-dipol array on that site has not been performed.

Topographic effect was included in resistivity models by marking all electrode positions with a Leica GPS differential static method. Average vertical and horizontal accuracy is respectively 0.05 and 0.02 m. During acquisition of the data only week current could be applied due to the high resistive ground. On the example of the Schlumberger array, despite the efforts to improve ground-electrode contact, only 63, 58 and 50% of measurements on profiles 3, 4 and 5, respectively, used the current over 5 mA. Minimum current possible to use was set to 1 mA. Although acquired data are characterized by high repeatability. Standard deviation higher that 5%, in the worst case for the Schlumberger and Wenner arrays, was possessed only by the 4% of measurements while for the dipol-dipol protocols it was below 7%. For the final processing, data sets has been cleared from the measurements that were too large or too small compared to their neighbouring data. Results of this process is placed under each resistivity model presented on subsequent figures. For the inversion procedure, the Res2Dinvx64 v.4.0. software was employed. Resistivity models on which the basic interpretation has been made originate from Schlumberger data sets. They are presented as the inset A on figures 4 to 6. Due to the weak currents that were employed during measurements for those resistivity models the absolute difference method, which attempts to minimize the difference of the first power between measured and calculated apparent resistivity values has been chosen (Loke *et al.* 2003; Loke 2014). For the search of resistivity distribution in those models the standard smoothness-constrained least squares method was used. All the other parameters and their factors in inversion procedure, were left on basic settings of this software version.

In applied methodology, on every data set, over 40 additional inversions with predefined parameters have been performed in order to test the stability of the solution search within models space. This allowed to emerge among all obtained resistivity models a few that were characterized by more realistic secondary features in terms of shape and size. It was partially connected with

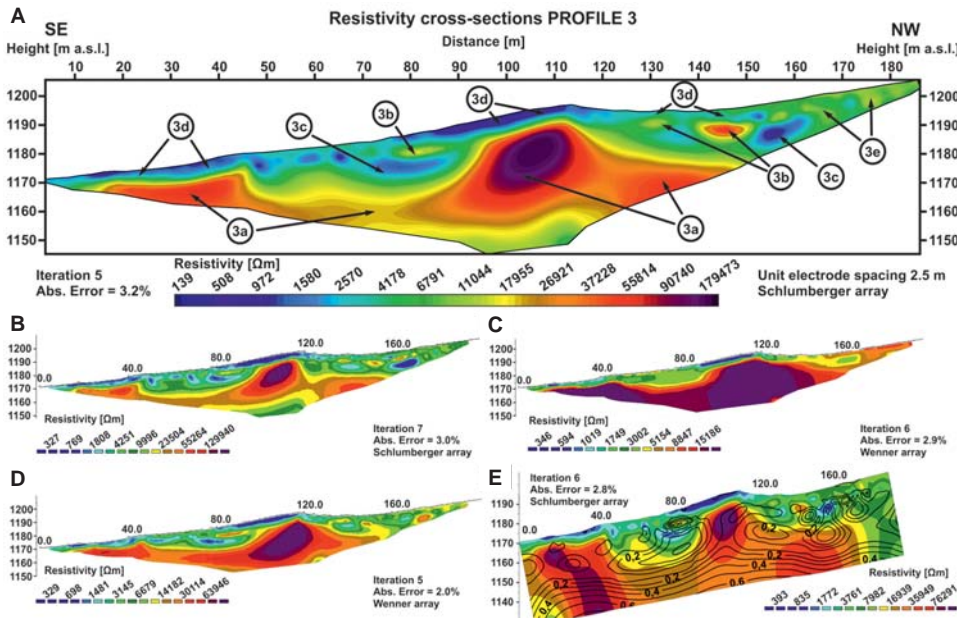


Fig. 4. Electrical resistivity tomography on the Storglaciären forefield, profile 3: (A) resistivity model selected for main interpretation, robust data constrain (RD) and standard model constrain SM (after Dobiński *et al.* 2017). note: the same color scale for A graph in Figs 4, 5, and 6; (B) Schlumberger array, RD, SM cutoff factor for data constrain (cffdc): 0.0001; (C) Wenner array, RD, Robust model constrain (RM) cutoff factor for data constrain: 0.1; (D) Wenner array, RD, SM, initial damping factor (iDF): 0.05, minimum damping factor (mDF): 0.005; (E) Schlumberger array with extended model discretization overlapped with DOI index map, interval of isolines: 0.1.

worsening of the overall structure but gave additional information to improve the geological interpretation of resistivity models, especially near the surface. Those few chosen models can be found on figures 4 to 6, insets B–D. Inversion parameters used for their creation are located in captions of figures 4–6.

To take into the consideration the reliability of prepared resistivity models, depth of investigation (DOI) index method has been used. It was proposed by Oldenburg and Li (1999) to empirically determine fragments of the model that significantly depends on parameters of the inversion. In principle it is based on comparing two cells of resistivity models created from the same data set using various values of the reference model and normalization of this difference. In places where the result depends strongly on data, DOI index will tend to near zero values, while in places where the parameters of objective function are strongly responsible for obtained resistivity it will rise up to 1.0. Results of DOI index calculations greatly supported the interpretation process of mountain permafrost studies (Marescot *et al.* 2003). Further use and modifications of DOI index method were presented also by Oldenburg and Jones (2007), Hilbich *et*

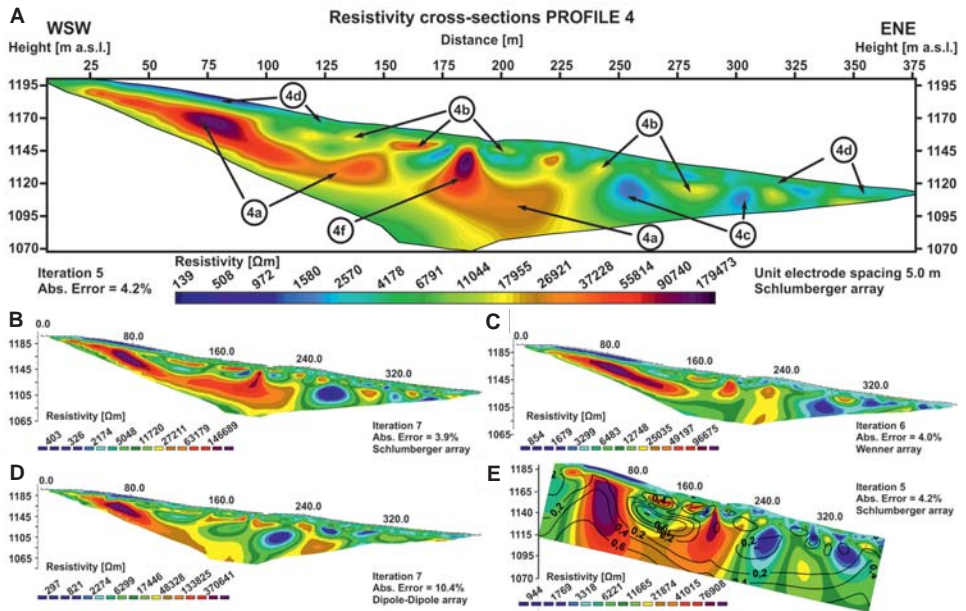


Fig. 5. Electrical resistivity tomography on the Storglaciären forefield, profile 4: (A) resistivity model selected for main interpretation, RD, SM (after Dobiński *et al.* 2017); (B) Schlumberberger array, RD, SM, iDF: 0.05, mDF: 0.005; (C) Wenner array, RD, SM, cffdc: 0.001; (D) Dipole-dipole array, RD, SM, cffdc: 0.0001; (E) Schlumberberger array with extended model discretization overlapped with DOI index map, interval of isolines: 0.2.

al. (2009), Caterina *et al.* (2013), and Deceuster *et al.* (2014). In application of DOI index method for obtained data 0.3 cut-off factor has been used. Detailed information on the applied DOI methodology has been described in Glazer *et al.* (2014). Calculation of this index requires extended discretization of the models up to minimum 3 times maximum depth range of array. For the practical reasons maps of DOI index in figures 4–6 in insets labelled as E, are cut. They are overlapped with the models originated from Schlumberberger protocol data.

Results and interpretation

Surveys conducted in the lower part of the Storglaciären forefield, were performed entirely outside the presently glacierized area, but in the place that was covered with the intense glaciation during the Pleistocene and the LIA (Fig. 1). The studied area is located at the altitude between 1075 and 1250 m a.s.l. *i.e.* above the lower limit of contemporary permafrost in this area. The first described 200 m long ERT profile 3 (Fig. 4) was carried out parallel to glacier front in the

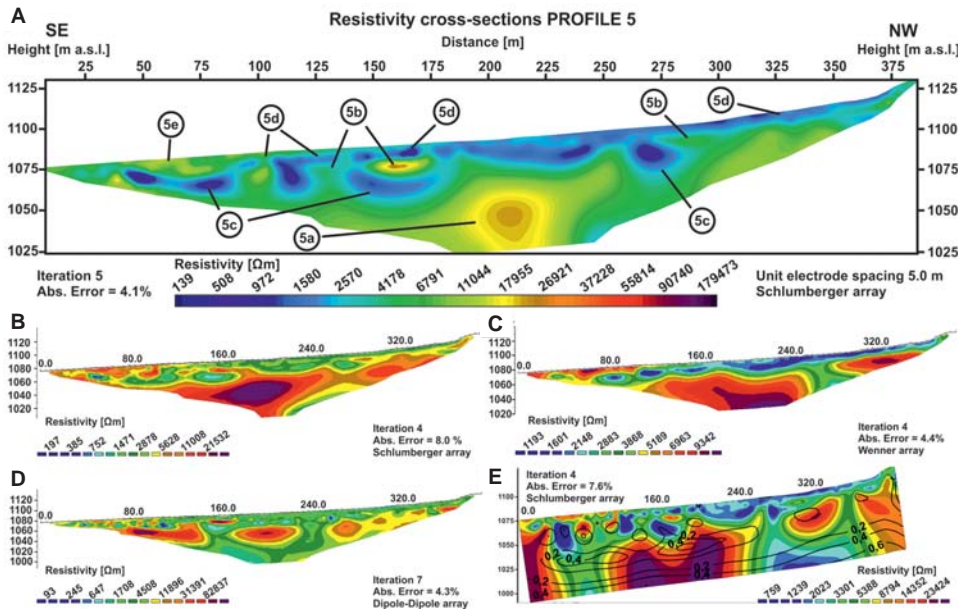


Fig. 6. Electrical resistivity tomography on the Storglaciären forefield, profile 5: (A) resistivity model selected for main interpretation, RD, SM; (B) Schlumberger array, RD, SM, vertical to horizontal flatness filter ratio (vhff): 0.5; (C) Wenner array, RD, SM, iDF: 0.15, mDF: 0.1; (D) – Dipole-dipole array, RD, SM, iDF: 0.05, mDF: 0.005; (E) Schlumberger array with extended model discretization overlapped with DOI index map, interval of isolines: 0.2.

youngest part of the glacier forefield. It is located on a fresh moraine material left by the glacier about 5–10 years ago. The profile 4 (Fig. 5) is perpendicular to the former and located on a relatively steep slope covered mostly with older, in upper part ice-cored morainic sediments of Storglaciären (Østrem 1964; King 1984; Kneisel 1999). The profile includes also material deposited here in the 1960–1980's. The third profile (profile 5, Fig. 6) is located on a flatter terrain, almost perpendicularly to the second one and in the area with more vegetation and water from streams draining that area. It is located at the bottom of the valley, inside the area of maximum glacier advance LIA (cf. Fig. 1). The glacier left this region in the 1940s (Fig. 1).

Profile 3. — In profile 3 (Fig. 4.), the 2.5 m spacing of electrodes at the distance of 200 m enables to reach the depth of *ca.* 45 m. Such an approach shows clearly the two types of high-resistivity anomalies which have diverse structure and resistivity values. The resistivity model is dominated by a large very high-resistivity one, with the upper uneven surface which is visible at the depth of *ca.* 5–17 m and the distance between 10 and 150 m (marked as 3a on Fig. 4A).

Its resistivity range from 20 to 180 k Ω m. The smaller, discontinuous anomalies, are located in the form of thinner layer, near the surface (marked as 3b on Fig. 4A), with resistivity of 10–40 k Ω m. The thickness of surface, water saturated layer is *ca.* 5 m (marked as 3d on Fig. 4A), except the last 30 m of the profile, where sediment material is more coarse and dry (marked as 3e on Fig. 4A). On the Fig. 4B, shallow high resistive layer (marked as 3b on 4A) obtains a more continuous shape of lenses in comparison with main resistivity model (4A). Furthermore, it is possible to designate the same structure horizon, at the places that previously have been incorporated into lying below high resistive massive body. It can be seen at the 60 and 130 metre of this profile. In case of structure labeled as 3a depending on inversion parameters, its uniformity can be easily obtained as it is shown in windows C and D using Wenner array. This behaviour suggest sudden change in nature of material between this structure and its cover. DOI map (Fig. 4E) suggest that lower parts of 3a anomaly where resistivity decreases, should not be treated as reliable. It is possible that this change does not reflect geological structure but artefacts of inversion process. Into consideration also should be taken the influence of three dimensional geological structure. In this case the layer of relatively high conductivity covering 3a body might for the large arrays prefer significantly more the horizontal dispersion of current instead its penetration with depth and thus providing misleading data. DOI index values seems to rise in areas of the contact between bodies with high resistivity contrast.

Profile 4. — The 4 profile (Fig. 5) was led downslope nearly perpendicularly to the previous one. It was performed with the electrode spacing of 5 m, which made it possible to attain the length of 400 m. In effect, its results can be interpreted down to the depth of *ca.* 80 m. The profile shows the high diversity of resistivity values found in the moraine material at this distance. It is worth to emphasise the specific stratification of high-resistivity anomalies, which are visible in the profile. The upper high-resistive discontinuous layer become visible at the distance of *ca.* 300 m of the profile with values *ca.* 20 k Ω m at depth between 4–7 m (marked as 4b on Fig. 5A). Below it, the possibility for water penetration still exists, and it is confirmed by lower resistivity values *ca.* 500–3000 Ω m (marked as 4c on Fig. 5A). Below, there is thick continuous and probably impermeable layer that has much higher resistivity values: between 20 and 170 k Ω m (marked as 4a on Fig. 5A). Use of low values of damping factors in inversion procedure allowed to enhance the 4b horizon (Fig. 5B). It is well developed almost along the entire length of the profile. This approach gave particularly good results at the 90 meter of profile where it could be separated from 4a structure. On resistivity models made by Wenner and dipole-dipole data, anomaly 4f does not extend to 4a structure. This part although on DOI index map for the main model possess very high reliability, it should not be considered as realistic feature. Data acquired in this area are characterized by good quality what in combination with the result

on resistivity model originated from Wenner array leads to conclusion that 4f anomaly might come from very specific, local structure conditions that shielded underneath potential distribution. For this fragment of geological medium, best representation on resistivity model would be by dipole-dipole data that gives here biggest absolute error in result. Analysis of DOI index on this profile suggest that no reliable information below 4a structure have been recovered. In the middle of the profile *ca.* 160 m length the interpretation should stop below 1100 m a.s.l. Just as it was in case of profile 3, DOI values rise on the contact between two resistivity structures. However, in this case this effect is enhanced by the bigger contrast and reduction of sensitivity below 4b lenses.

Valley bottom – Profile 5. — The 5 Profile (Fig. 6) is located at *ca.* 100 m lower elevations than the profile 3. It was performed at the bottom of the valley, in the area occupied by the glacier during the LIA First 140 m of its length is located in a slightly drier area, which protrudes a bit over the surroundings. Further on, the area is moist and partially marshy, because terrain is relatively flat and the superficial drainage is not intensive. The changing terrain conditions affect the resistivity of the upper layer. At the beginning, the resistivity of surface layer reaches 15 k Ω m (marked as 5e on Fig. 6A), but then – after the 125 metre, it drops to *ca.* 0.5–2.5 k Ω m (marked as 5d on Fig. 6A). Its thickness is *ca.* 6–12 m. Although they rarely occurring and possess much smaller spatial dimensions there is still possible to distinguish horizon associated with the relatively high resistivity lenses (marked as 5b on Fig. 6A). Locally low-resistivity anomalies, most probably indicating a deeper water penetration, reaching 20–30 m under the ground surface (marked as 5c on Fig. 6A). Underneath, a distinct thick and uneven layer of high resistivity, reaching 25 k Ω m, is detected (marked as 5a on Fig. 6A). In the window B where in resistivity model the horizontal structures have been preferred, the 5b horizon tends to emerge in stable structure up to 190 m. It can also be observed, although in weak form and a little shallower, between 280 m and end of the profile. Presented resistivity model originated from Wenner data is characterized by low resolution. It tends to generalize geological medium only to main structures. Therefore it underlines the different nature between low resistivity sediments and high resistivity anomalies underneath. Model from dipole-dipole array data distinguish well the 5b lenses. It additionally confirms the character of its composition. In case of 5a high resistive anomalies, their discontinuous nature has been highlighted. For their depth extent estimation similar discussion as in the case of profile 3 should be undertaken. Especially when low damping factors has been used which could strengthen considered effect. DOI index also in this case tends to rise on the contacts of bodies with high resistivity contrast. Beyond these fragments, it has stable distribution.

Discussion

First of all, results of our research confirms previous findings of a large high-resistivity anomaly in the moraine located in the immediate vicinity of the glacier, which is interpreted as dead ice blocks (Østrem 1964; King 1984; Kneisel 1999). Due to the previously reported permafrost occurrence in this area at the depth of 2 to 4 metres below active layer the synthetic modelling was used to verify the results showed in resistivity models that use arrays with larger electrode spacing. For that purpose Res2Dmod software was applied. Constructed model assume discretized layers that the depth to their successive bases near the surface is at 2, 4, 6, 9, 12 *etc.* metres. This allowed to model high resistivity lenses with various thickness at the expected depth of permafrost table. Furthermore the high resistivity monolithic structure, with uneven permafrost table such as it is observed on profile 3 (unit 3a in Fig. 4A), was added at the bottom of the model to test its behaviour. For the acquisition of synthetic data Schlumberger protocol with 5 m electrode spacing was used. The specification and amount of data acquired in this step was set to reconstruct the settings from used Terrameter LS protocol. No noise was added to measurements. Both: model and the result of the inversion using the same parameters as the main interpreted resistivity models presented in Fig. 7.

Analysis of the results of the synthetic modelling shows that: 1) Due to the minimum electrode spacing which has similar size as the active layer thickness, the resulting model develop permafrost table at the slightly larger depth. It is the consequence of relatively low geophysical information available within this near surface layer and discretization of cells in resulting model; 2) Despite the fact that high resistivity structure at the lower part of the synthetic model was uniform as a result, heterogeneous anomaly has been obtained. This effect is related to lowering of the structures roof between two upthrusts and filling of this space with relatively high conductive formations. As the result, the measurements over such structure do not contain much information over deeper resistivity distribution.

The upper, low resistivity surface layer marked as “d” is the permafrost active layer in each case (Fig. 4: 3d; Fig. 5: 4d; Fig. 6: 5d). Below it, close-to-surface high-resistive usually discontinuous layers labelled with “b” correlate very well with each-other and can be interpreted as contemporary permafrost which was formed after the glacier retreat, but its development could start also under the cold-based glacier tongue (Dobiński *et al.* 2017). This statement is supported by the constant thickness of the “d” layer over “b” lenses which can be observed regardless of the location of the measurement: direct vicinity of the glacier forehead (profile 3), steep slope (profile 4), long deserted glacier forefield (profile 5). Research shows that at the depth of several to several dozen metres there is another much larger high-resistivity anomaly that reach 20–190 k Ω m. It is labeled on models as an “a”. On profile 3 (Fig. 4: 3a) and beginning

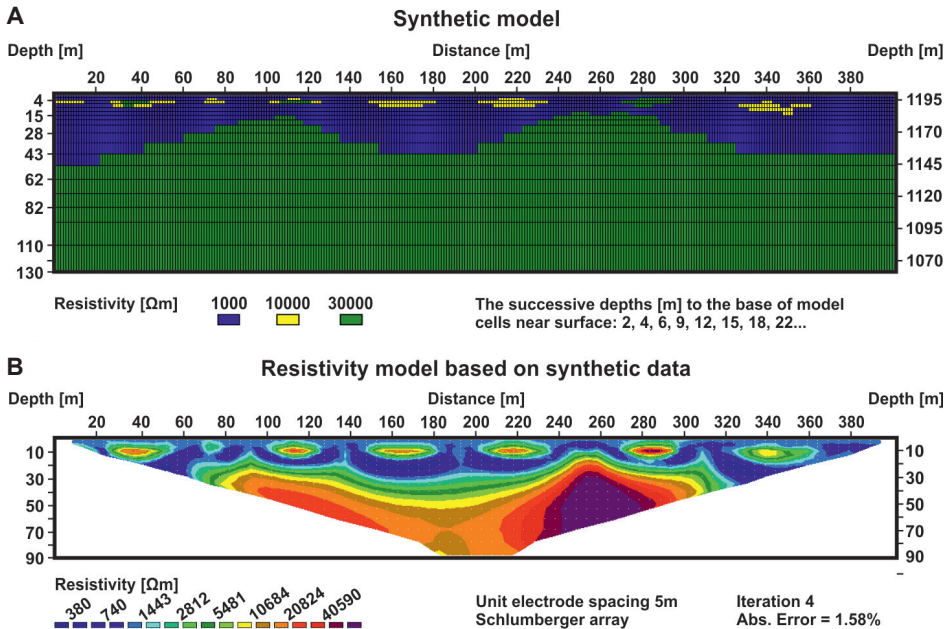


Fig. 7. Synthetic model of permafrost occurrence in the research area, (A) Synthetic model, (B) Resistivity model generated from forward modeling for the structure in window A. The same inversion parameters has been applied as in the case of main models in Figures 4–6.

of profile 4 (unit 4a in Fig. 5) it reaches almost the surface. It is specific that stratum located above previously interpreted as an active layer also appears with the same constant thickness. It is the proof of the thawing process that affects those structures in the surface layer. Depending on interpretation, resistivity values can be considered as indicative of ice-rich permafrost or a buried ice probably glacial ice core, remaining from the retreating glacier (Østrem 1964). Due to the high resistivity nature of this structure the deepest parts of models are featured with little credibility as DOI index supports that. Also, doubts associated with unknown size of the effect of three dimensional structure and potentially possible error connected with possibility of horizontal flow of electric current during the measurement, not allow for drawing substantial conclusions based on that part of models. Beginning and centre part of profile 3 (Fig. 4A) as well as the first 120 metres of profile 4 (Fig. 5A) lies at the preserved parts of diamicton plain. Other surface sections of the profiles are located mostly at the abandoned by glacier but modified by glacial drainage terrain, according to sediment–landform associations in the proglacial area of Storglaciären (Etienne *et al.* 2003). Glacifluvial activity can be visible also on profile 4 (Fig. 5A) in its middle part, passing Nordjåkk stream (narrow trench orientated NW–SE) and in the first 100 m of profile 5 (Fig. 6A).

Almost entire Storglaciären forefield is located on the Tarfala Amphibolite geological unit, and yet the distinction between bedrock and superficial sediment cover is problematic on resistivity models. Firstly, the trench on profile 4 mentioned before, with NW–SE orientation and linear position nearly perfectly corresponds with the two outcrops of amphibolites in the south east direction, suggesting that substantial erosion made by Nordjåkk in this place cutting this geological structure. This implies existence of very thin sediment cover which is not suggested by obtained resistivity models. Secondly on profile 3 the continuity of “a” near surface anomaly can be observed but not in the shape of two upthrusts. Third, the contacts between deeper resistivity complexes are characterized by big and sharp contrast. In case of bedrock in forefield, there should be rather smooth change in resistivity as the cracks present on upper part gradually decrease with depth. Noteworthy is the fact that “d” cover over “a” structure is wider than its upthrusts. For this reason, we interpret the lower high resistivity structure as permafrost in state of degradation caused also by the meteoric water. Such conclusion is supported also by correlation of low resistivity anomalies “c” at the depth up to 30 m below surface, with the glaci-fluvially-modified terrain. It is especially well noticeable relationship between 50 to 90 m of profile 3 (Fig. 4A) where on surface at this distance inactive channels have been observed. Anomalies “b” and “d” also occur on profile 5 (units 5b and 5d in Fig. 6). In case of “a” structure, it is most probably the occurrence of permafrost in amphibolite bedrock but it is problematic to definitely designate the beginning of its intact structure.

Thus, it is very likely that in the research area we are dealing with permafrost of two types. Near-surface permafrost, the genesis of which has to be associated with the current climate which forms a discontinuous layer several metres thick (*ca.* 2–4 m) at the depth of *ca.* 3–4 m under the ground surface. The resistivity values inside are diverse and they are significantly influenced by the ablation water from the glacier front. It probably rests on the permeable talik located beneath. The ice inside this permafrost layer may be created as a result of freezing of meteoric and ablation water (Kneisel 1999). Below there is also a discontinuous layer of much lower resistivity, which does not imply such freezing. Inside it the drainage of ablation water and, to a lower extent, precipitation water may occur. Both layers have an uneven course. At the depth of several metres near the glacier and dozen metres from the front, there is another very distinct, large high-resistivity anomaly. It is considerably thick and overcome the ERT measurement range, here *ca.* 50 m in the 200 m profile (Fig. 4) and over 80 m in the perpendicular 400 m profile (Fig. 5). It may be interpreted as older permafrost without relationship to the current climate, with possible occurrence of some underground ice, as well as “dry permafrost” which can probably exist at considerable depth.

Those two permafrost layers also may occur in the lower part of the glacier forefield, where the occurrence of contemporary permafrost is less obvious

(Fig. 6). Such two-layered permafrost occurrence in this area is suggested also by King (1984). This upper permafrost layer, linked to the current climate and susceptible to the influence of water in the summer period, may be discontinuous and of highly diverse thickness. As stated above deeper located layer is obviously much less susceptible to the influence of the contemporary climate. Due to geological structure of the area, the character of glacial sediments, water drainage and its course is diverse as well. The presented longer and deeper ERT profiles provide a much better and complete presentation of permafrost found in the Storglaciären forefield in comparison with previous research (King 1984; Kneisel 1999).

Based on the conducted geophysical research and previous studies, a new model of permafrost aggradation on the the area of the Storglaciären and its forefield may be proposed. It is based on the variable cold penetration within the lithosphere during the time. At the beginning frost penetrates the upper, cold-ice layer of the retreating glacial tongue to several, or even several dozen metres. The glacier tongue freezes up to the ground in the lower, thinner part of the glacier, which allows cooling of the ground underneath, and subsequent frost penetration of this ground. The formation of permafrost layer at the glacier front is hindered due to seasonal air temperature variation and glacial ablation, which degrade partly the frozen ground in the forefield by water of glacier ablation, snowmelt, and by positive summer temperatures. Because of activity of these agents, the upper permafrost layer is most probably discontinuous and not very thick (down to several metres). Between the glacial tongue and forefield, there occurs specific continuous transition from subglacial permafrost and accompanying cold glacial margin to periglacial permafrost which exists in the glacier forefield. The “periglacial” permafrost has a dual, two-layered character as was stated above. The upper layer is discontinuous permafrost of genesis linked with the current climate. Underneath, there is permafrost which is more uniform and which seems to be much older.

For the full picture of permafrost occurring in the vicinity of the Storglaciären, it is worth to mention the possibility of the permafrost occurrence especially in the highest localized scree slopes. There are certainly climatic conditions favourable for the occurrence of syngeneic permafrost associated with the accumulation of ice in the sediment material. Its aggradation may be associated with the occurrence of the so-called *chimney effect* (e.g., Sawada *et al.* 2003; Delaloye and Lambiel 2005; Scapozza *et al.* 2011) which may also occur in such conditions.

The climatic variability in the Holocene influenced the shape, evolution, and temperature of permafrost although it happened with a delay. In order to define its climatically-induced evolution in general, the most adequate is to associate it in wider scale, with the evolution of arctic permafrost, which in analogical way is most evident in the western part of Siberia. The variability of the permafrost range in both: mountain and Arctic environments should be linked with the

same global climatic variability in the postglacial period. In the flatlands of West Siberia, this variability was characterized by a horizontal shift of climatic zones while in the mountains analogous variability of altitudinal climatic belts was vertical. This analogy was adopted as the hypothesis of this study.

Geophysical model of mountain permafrost occurrence in the Tarfala area. — The obtained empirical data allow us to propose also a new general geophysical model of the permafrost occurrence in the mountainous environment, which better reflects climatic changes which influenced permafrost evolution and may have therefore broader and more universal application (Dobiński 2011b). To make it possible, results of studies from other mountainous areas together with other published concepts of permafrost occurrence were employed as well. The authors also aim to find and correlate joint solutions allowing to explain the analogous shape and geophysical character of mountain and Arctic permafrost.

The following data were used to compile this model: (1) Results of ERT geological studies conducted by the authors; (2) Published results of studies on permafrost in Scandinavia and especially, the Tarfala area; (3) Model of and information on the permafrost occurrence character in the Ylläs Mts, northern Finland; and (4) Model of and information on the permafrost occurrence in West Siberia. The information on items 1 and 2 have already been presented.

Model of permafrost occurrence in the Ylläs Mts, Finland. — The publication which in details describes the manner of occurrence and evolution of mountain permafrost in northern Scandinavia by means of numerical modelling is the study published by Kukkonen and Šafanda (2001). The one-dimensional general model for northern Fennoscandia was compiled on the basis of paleoclimate data calculated for the Sodankylä station (67°22'N; 26°38'E; 180 m a.s.l.) up to 6000 years back. The mean annual air temperature in this station was -0.97°C in from 1971 to 1990, so it is close the mean annual air temperature in the Abisko, located near the Tarfala area (*ca.* 400 m a.s.l., MAAT -0.9°C). The mechanism of permafrost formation and degradation in the Ylläs Mts, was calculated for the following data: ground temperature value: -2°C, temperature gradient: 8 mK m⁻¹ and porosity: 5%. The initial permafrost thickness in the model was calculated to be 266 m (with 5% porosity). In the Atlantic period, the permafrost degradation resulted in its thickness dropping to *ca.* 190 m, and the cooling that followed made it thicker again (Kukkonen and Šafanda, 2001). The difference in permafrost occurrence for the model with 5% and 0% porosity is shown in Fig. 8. The modelling-related distribution of current ground temperatures in those mountains is illustrated in Fig. 9.

The Ylläs, small mountain range, is located *ca.* 260 km to EES from Tarfala and *ca.* 100 km to WNW from Sodankylä. The maximum height of these mountains is 712 m a.s.l. The mean annual air temperature in this region

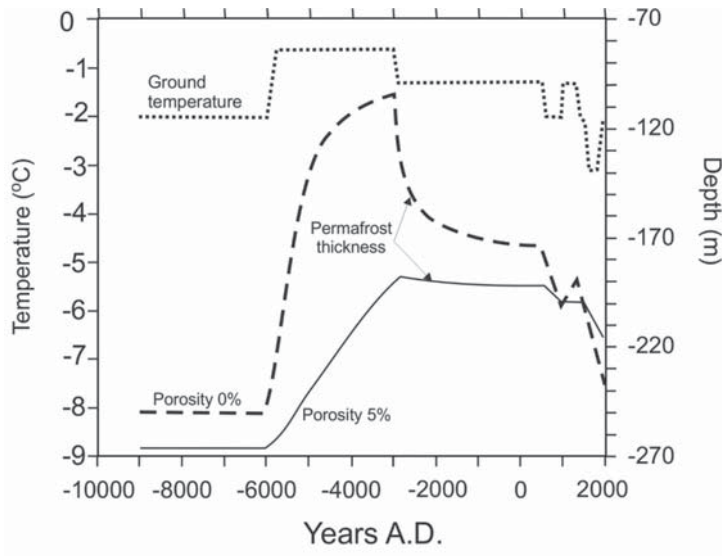


Fig. 8. Variation of permafrost thickness during the Holocene in the Ylläs Mts Northern Finland, after Kukkonen and Šafanda, 2001, fig. 5 (modified). See this publication for further details.

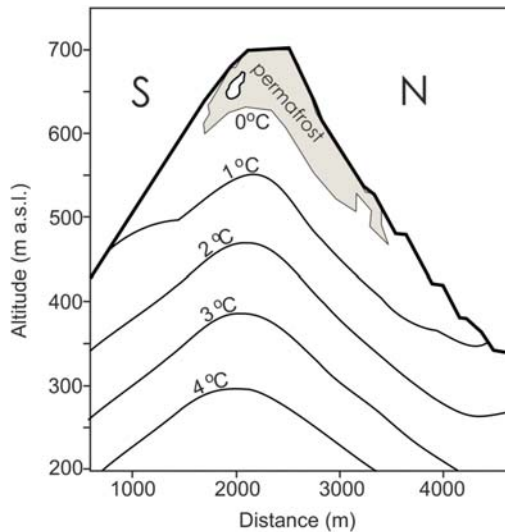


Fig. 9. Results of two-dimensional transient simulation of bedrock permafrost in the Ylläs Mts – the present temperature, after Kukkonen and Šafanda, 2001, fig. 8 (modified). See this publication for further details.

of Lapland ranges from -1 to -2°C , which means that at the height of 700 m a.s.l. it should be around -4 to -5°C . These values are fully comparable to the air temperatures in the Tarfala region. The -0.6°C value has been accepted as the current ground temperature in the highest peak of the Ylläs Mts. It may be inferred from the conducted modelling that the highest places with northern exposure were not subjected to any conditions allowing the complete degradation of permafrost during the entire Holocene. Conical shape of permafrost layers visible asymmetrically on the N and S slopes are the result of interaction between atmospheric and geothermal heat flow. This “geophysical shape” should be supplemented by the sequence of layers which reflects the climatic evolution of permafrost.

Permafrost model in West Siberia. — The last element necessary for model construction comes from model of permafrost occurrence in West Siberia. Dostovalov and Kudriavcev (1967) are probably the first to describe it. The permafrost of that region developed originally as a result of cold climate linked to the Pleistocene cooling and characteristic continentalism of that area. Generally, permafrost thickness decreases towards the south, which leads to its range changing in the same direction, going from the zone of continuous permafrost, through discontinuous, sporadic, and isolated patches. However, both: the thickness, and range of individual zones fluctuated periodically, influenced by changing climate. Periodical coolings were associated with the aggradation of all permafrost zones towards the south and an increase in their thickness. Warming, on the other hand, caused the thickness to degrade gradually, which occurred both on the top as a result of climate influence and on the bottom, resulting from geothermal gradient. The process finally led to the formation of a layer of permafrost which lost a direct contact with the active layer. Such permafrost is referred to as inactive or fossil.

Climate warming does not necessarily lead to the total degradation of permafrost as it does not last long enough, as it is visible in the West Siberia. The permafrost may hold for a long time even at a substantial depth, being isolated from short-lasting climate changes by a relatively thick layer of ground, which absorbs and delays those changes. The next intense climate cooling leads to the formation of a new permafrost layer at the surface as an effect of that cooling. Near the southern permafrost border in West Siberia, these layers occur separately, forming two semi-parallel layers of permafrost. Their thickness increases towards the North along with the intensification of climate severity until they overlap, forming one permafrost layer without talik. Their genetic variety may be seen in the temperature profile, which is not rectilinear but shows temperature fluctuations illustrating climate changes, naturally in the scope of negative temperatures (cf. fig. 9 in Dobiński 2011a).

Russian scientists, studying these two different permafrost layers determined that the upper layer comes from the Holocene and the lower one from the Pleistocene. The former exhibits the thickness of *ca.* 50 m, is discontinuous and can be found between 66°–64°N. The latter, found below, is separated by talik 100–200 m thick. That layer reaches parallel 60°N. Its occurrence has been proved by boreholes (Astakhov 1995; Ananajeva-Malkova *et al.* 2003). It is a relict permafrost, remnant of the Pleistocene cooling, which in the late Vistulian glaciation reached 51°N, *i.e.* 1500–1600 km further to the south. The talik occurring in-between is treated as an effect of degradation during the Holocene climatic optimum. (Baulin 1982; Yershov 1992; Heginbottom 2002). The views on its genesis and evolution are reviewed in more detail by Astakhov (1995). He claims that, apart from the Holocene warming, there were no climate fluctuations that could reach deeper than several dozen metres. The permafrost occurrence in West Siberia is illustrated on a diagram in Fig. 10.

Based on our results, and publications of similar results obtained from other mountainous areas in Europe and based on the existing analogies, a hypothesis may be suggested that the occurrence of mountain permafrost in the Tarfala region consists of the models proposed by Kukkonen and Šafanda (2001) and Dostovalov and Kudriavcev (1967). A conical shape, corresponding to mountain slope inclination, and altitudinal variability of the transition from sporadic to continuous permafrost is analogous with the model for West Siberia, where permafrost may occur in two layers, as it has been characterised above, *i.e.* as active, contemporary permafrost corresponding to the current climate and inactive, fossil permafrost formed during the previous climatological/geological

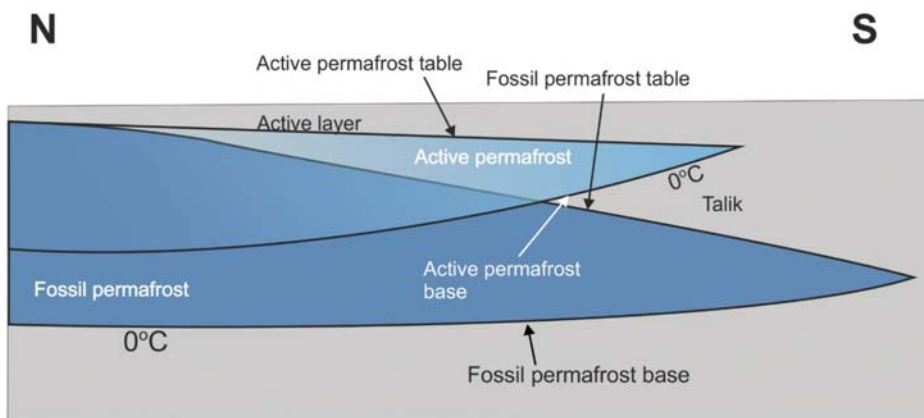


Fig. 10. General conceptual model of the permafrost occurrence in the Western Siberia after Dobiński 2011b (modified).

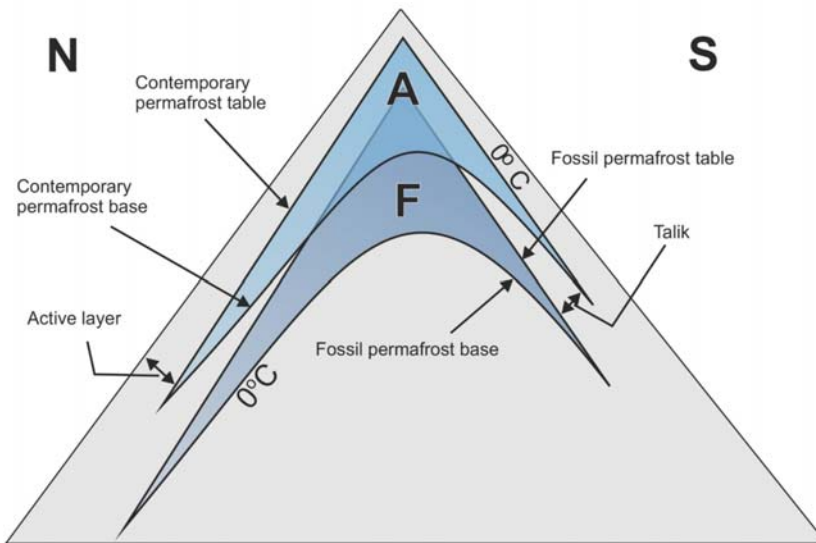


Fig. 11. Conceptual model of mountain permafrost occurrence in the area of Kebnekaise, and surrounding mountains, after Dobiński 2011b. A – active, contemporary permafrost, F – fossil, older, inactive permafrost (modified). Permafrost zones (continuous, discontinuous, sporadic) are not included in the model due to its simplicity.

periods. In these mountain areas, the layers may overlap in a way that may hinder their differentiation; lower, they may occur separately (Fig. 11). The layer of deeper fossil permafrost can be found at lower altitudes and greater depth. It may be covert, encompassing solid, dry rock, and does not have to show on the surface in any specific landforms *e.g.* patterned ground, ice-wedge polygons, sorted circles, pingos etc. (Black 1976). The variety of permafrost occurrence depends on climate changes which took place in the past, most probably after the glaciation has retreated, although the aggradation of permafrost in the ground could have started even prior to complete glacial retreat (Kneisel 1999).

Then the evolution of permafrost in some mountainous regions may be illustrated by application of this model. It pertains to those mountains ranges where climatic fluctuations and change in local glaciation were noted. Apart from the Scandinavian Mts, it is highly probable that this may be applied to the Tatra Mts and Alps as well. The general model of two-layer mountain permafrost is shown in Fig. 11.

As mentioned above, in the first Holocene stage or even in the late Pleistocene, the influence of cold glacial/periglacial climate led to a very deep frost penetration of lithosphere in the mountains, which may have created permafrost of 400–500 m thick in the Tatras (Czudek 1986), 600 m thick in the Scandinavian

Mountains (Gorbunov 2003), and even 1000 m thick in the Alps (Haeberli and Funk 1991). Gradual warming of climate in the Holocene led at first to the stabilisation of thermal balance, then to its reversal and permafrost degradation at the end. The process began at the lowest altitudes: first in mountain valleys, and as the warming proceeded, the permafrost degradation encompassed higher areas. In the late Pleistocene and early Holocene permafrost in lower located areas (valleys) began to degrade, but in the high mountains, such as the Alps, Scandinavian Mts or Tatra Mts, the climate warming in the highest mountainous ridges never reached temperatures above zero MAAT. There and in those lower places where the temperature was above zero for too short periods permafrost could hold at considerable depths. Another cooling caused the degradation to stop, thermal balance to reverse again and, at proper heights, permafrost to aggrade anew (Dobiński 2011b).

The degradation, *i.e.* gradual disappearance of permafrost, is always preceded by an increase in its temperature. At the altitudes where the ground temperature did not rise above zero, permafrost did not degrade completely, but merely changed its thermal properties (increase of its temperature). That change could be detected only by means of the direct method, *i.e.* the measurement of temperature in a borehole at various depths. Analogous data may be obtained when employing the ERT method. The re-aggradation of permafrost acts in the reversal direction. This led over time to the formation of new, current climate-related permafrost layer (Fig. 11). Two-layered permafrost probably exists in other mountain ranges, as indicated by the results of the studies related to its and its associated forms, such as rock glaciers (Ødegård *et al.* 1996; Hauck 2001; Isaksen *et al.* 2002; Hauck *et al.* 2004; Ikeda 2006; Kneisel 2010; Krainer *et al.* 2015).

Conclusions

Results of ERT surveys and publication studies allow to connect on the basis of analogical climatic changes two types of permafrost, which was seen separately, and unify its evolution in mountainous and Arctic regions in a uniform way. In both cases, climate evolution influences the “permafrost shape”, as a climatic “product”. Holocene climatic changes most probably allow for formation of two permafrost layers connected with two different periods of cooling separated with a warmer period. These layers may overlap, especially in places where degradation of the older layer due to height increase is slight and aggradation of the younger layer penetrated deeper, or in case of dead glacial ice core. Horizontal regularity found in Western Siberia takes an analogous vertical form of slope inclination in the mountain environment, adjusting to the relief. Horizontal climatic variability is also replaced by vertical variability.

Occurrence of permafrost in the studied region outside the glacial environment can be divided into:

- Contemporary permafrost, with genesis corresponding to the current climate of the area. Its depth reaches several metres and it is mostly of non-continuous. It can also contain polygenetic ice in a relatively high amount. It can originate from freezing rain, snow patches, glacier dead-ice, and freezing of glacial ablation water;
- Fossil permafrost which is located underneath contemporary permafrost at the depth of several–several dozen metres. It was created as a result of cold climate impact previously present in this area for long time. It can contain some ice, but in a lower amount than contemporary permafrost, probably is partially formed of weathered material, but may include also solid rock located under these deposits: dry permafrost.

The noted regularities can also occur in other mountain massifs and ranges. Attempts to discover two (or more)-layered permafrost in other mountain regions of the world where climate evolution in the post-glacial period is known, can be the goal of further studies on mountain permafrost. Such works will allow to document its presence better and identify the arising consequences for determination or revision of its range on a global scale, and in mountainous geomorphological processes.

Acknowledgements. — This article is one of the results of a research project funded by the National Science Centre, Poland (NCN) DEC-2012/07/B/ST10/04268. Sincere gratitude goes to Mariusz Grabiec who helped in fieldwork research. Tarfala Research Station, Stockholm University, is acknowledged for field work assistance and meteorological data provided. Stuart Harris, Petru Urdea and anonymous reviewer is acknowledged for his helpful suggestions, Monika J. Fabiańska helped with the manuscript language editing. AMDG.

References

- ANANAJEVA-MALKOVA G.V., MELNIKOV E.S. and PONOMAREVA O.E. 2003. Relict permafrost in the central part of Western Siberia. *In*: Phillips M., Springman S. and Arenson L. (eds) *Permafrost*. ICOP Zurich: 5–8.
- ANDRÉASSON P.G. and GEE D.G. 1989. Bedrock geology and morphology of the Tarfala area, Kebnekaise Mts, Swedish Caledonides. *Geografiska Annaler* 71A: 235–239.
- ASTAKHOV V.I. 1995. The mode of degradation of Pleistocene permafrost in West Siberia. *Quaternary International* 28: 119–121.
- ÅKERMAN H.J. and MALMSTROM B. 1986. Permafrost mounds in the Abisko area, Northern Sweden. *Geografiska Annaler* 68A: 155–165.
- BAIRD G.B. 2005. On the Bedrock Geology of the Tarfala Valley: Preliminary results of 2003 and 2004 fieldwork. *In*: Jansson P. (ed.) *Tarfala Research Station Annual Report, 2003–2004*, 2B (1): 1–5. Stockholm University, Stockholm.

- BAULIN V.V. 1982. *Map of the zonation of the West Siberian Plain based on the structure and thickness of the permafrost layer. (1: 1 500 000).*, USSR State Committee for the Council of Ministers of the USSR, Industrial and Scientific Research Institute for Engineering Surveys in construction, Moscow.
- BENN D.I. and EVANS D.J.A. 1998. *Glaciers and Glaciations*. Arnold, London. 734 pp.
- BLACK R.F. 1976. Features indicative of permafrost. *Annual Review Earth and Planetary Sciences* 4: 75–94.
- CATERINA D., BEAUJEAN J., ROBERT T. and NGUYEN F. 2013. A comparison study of different image appraisal tools for electrical resistivity tomography. *Near Surface Geophysics* 11: 639–657.
- CHRISTIANSEN H.H., ETZELMÜLLER B., ISAKSEN K., JULIUSSEN H., FARBROT H., HUMLUM O., JOHANSSON M., INGEMAN-NIELSEN T., KRISTENSEN L., HJORT J., HOLMLUND P., SANNELA B.K., SIGSGAARD C., ÅKERMAN H.J., FOGED N., BLIKRA L.H., PERNOSKY M.A. and ØDEGÅRD R.S. 2010. The thermal state of permafrost in the Nordic Area during the International Polar Year 2007–2009. *Permafrost and Periglacial Processes* 21: 156–181.
- CZUDEK T. 1986. Pleistocenni permafrost na uzemi Československa. *Geograficky Časopis* 38: 245–252. [in Czech].
- DAHLIN T. 2001. The development of DC resistivity imaging techniques. *Computers and Geosciences* 27: 1019–1029.
- DAHLKE H.E., LYON S.W., STEDINGER J.R., ROSQVIST G. and JANSSON P. 2012. Contrasting trends in floods for two sub-arctic catchments in northern Sweden – does glacier presence matter? *Hydrology and Earth System Sciences* 16: 2123–2141.
- DECEUSTER J., ETIENNE A., TANGUY R., NGUYEN F. and KAUFMANN O. 2014. A modified DOI-based method to statistically estimate the depth of investigation of dc resistivity surveys, *Journal of Applied Geophysics* 103: 172–185.
- DELALOYE R. and LAMBIEL C. 2005. Evidence of winter ascending air circulation throughout talus slopes and rock glaciers situated in the lower belt of Alpine discontinuous permafrost (Swiss Alps). *Norsk Geografisk Tidsskrift* 59: 194–203.
- DOBIŃSKI W. 2010. Geophysical characteristics of permafrost in the Abisko area, northern Sweden. *Polish Polar Research* 31: 141–158.
- DOBIŃSKI W. 2011a. Permafrost. *Earth-Science Reviews* 108: 158–169.
- DOBIŃSKI W. 2011b. *Permafrost occurrence in selected areas of the Tatra Mts., Scandinavian Mountains and Spitsbergen in the light of comprehensive geophysical research and climatological analyzes*. Prace Naukowe Uniwersytetu Śląskiego, 2850. 172 pp. [in Polish].
- DOBIŃSKI W. 2012. The cryosphere and glacial permafrost as its integral component. *Central European Journal of Geosciences* 4: 623–640.
- DOBIŃSKI W. 2017. Permafrost – definition and extent. In: Richardson D., Castree N., Goodchild M.F., Kobayashi A., Liu W., Marston R.A., (eds) *The International Encyclopedia of Geography*. John Wiley & Sons, Ltd: 1–9.
- DOBIŃSKI W., GRABIEC M. and GADEK B. 2011. Spatial relationship in interaction between glacier and permafrost in different mountainous environments of high and mid-latitudes, based on GPR research. *Geological Quarterly* 55: 15–27.
- DOBIŃSKI W., GRABIEC M. and GLAZER M. 2017. Cold – temperate transition surface and permafrost base (CTS–PB) as an environmental axis in glacier–permafrost relationship, based on research carried out on the Storglaciären and its forefield, northern Sweden. *Quaternary Research* 88: 551–569.
- DOSTOVALOV B.N. and KUDRIAVCEV W.A. 1967. *Obshtsheye merzlotovedeniye*. Izdatielstvo Moskovskogo Universiteta. Moskva, 257 pp. [in Russian].

- EKMAN S. 1957. Die Gewässer des Abisko – Gebietes und ihre Bedingungen. *Kungliga Svenska Vetenskapsakademiens Handlingar* 6: 1–172.
- ETIENNE J., GLASSER N., and HAMBREY M.J. 2003. Proglacial sediment-landform associations of a polythermal glacier; Storglaciären, Northern Sweden. *Geografiska Annaler* 85: 149–164.
- FUCHS M. 2013. *Soil Organic Carbon Inventory and Permafrost Mapping in Tarfala Valley, Northern Sweden. A first estimation of the belowground soil organic carbon storage in a sub-arctic high alpine permafrost environment*. Department of Physical Geography and Quaternary Geology, Stockholm University, Master's thesis NKA 75, Stockholm, 109 pp.
- GISNÅS K., ETZELMÜLLER B., FARBROT H., SCHULER T.V. and WESTERMANN S. 2013. CryoGRID 1.0: Permafrost Distribution in Norway estimated by a Spatial Numerical Model. *Permafrost and Periglacial Processes* 24: 2–19.
- GISNÅS K., WESTERMANN S., SCHULER T.V., MELVOLD K. and ETZELMÜLLER B. 2016. Small-scale variation of snow in a regional permafrost model. *The Cryosphere* 10: 1201–1215.
- GLAZER M., MENDECKI M.J. and MYCKA M. 2014. Application of DOI index to analysis of selected examples of resistivity imaging models in quaternary sediments. *Studia Quaternaria* 31: 109–114.
- GORBUNOV A.P. 1988. The alpine permafrost zone of the USSR. In: Senneset K., (ed.) *Proceedings, Fifth International Conference on Permafrost, Vol 1*. Tapir Publishers, Trondheim: 154–158.
- GORBUNOV A.P. 2003. *Wietchnaya merzłota gor. Ot ekvatora do poliarnych shirot*. Al'maty 122 pp [in Russian].
- HAEBERLI W. and FUNK F. 1991. Borehole temperatures at the Colle Gnifetti core-drilling site, (Monte Rosa, Swiss Alps). *Journal of Glaciology* 37: 37–46.
- HARRIS C., HAEBERLI W., VONDER MÜHLL D. and KING L. 2001. Permafrost Monitoring in the High Mountain of Europe: pace project in its Global Context. *Permafrost and Periglacial Processes* 12: 3–11.
- HARRIS S.A. 1981. Climatic relationships of permafrost zones in areas of low winter snow-cover. *Biuletyn Peryglacjalny* 28: 227–240.
- HARRIS S.A. 1982. Distribution of zonal permafrost landforms with freezing and thawing indices. *Biuletyn Peryglacjalny* 29: 163–182.
- HAUCK C. 2001. *Geophysical methods for detecting permafrost in high mountains*. PhD thesis, Laboratory for Hydraulics, Hydrology and Glaciology (VAW), ETH Zürich, Switzerland. VAW-Mitteilungen: 171 pp.
- HAUCK C. 2013. New concepts in geophysical surveying and data interpretation for permafrost terrain. *Permafrost and Periglacial Process* 24: 131–137.
- HAUCK C., ISAKSEN K., VONDER MÜHLL D. and SOLLID J.L. 2004. Geophysical Surveys Designed to Delineate the Altitudinal Limit of Mountain Permafrost: an Example from Jotunheimen, Norway. *Permafrost and Periglacial Processes* 15: 191–205.
- HEGINBOTTOM J.A. 2002. Permafrost mapping: a review. *Progress in Physical Geography* 26: 623–642.
- HILBICH C., MARESCOT L., HAUCK C., LOKE M.H. and MAUSBACHER R. 2009. Applicability of electrical resistivity tomography monitoring to coarse blocky and ice-rich permafrost landforms, *Permafrost and Periglacial Processes* 20: 269–284.
- IKEDA A. 2006. Combination of Conventional Geophysical Methods for Sounding the Composition of Rock Glaciers in the Swiss Alps. *Permafrost and Periglacial Processes* 17: 35–48.
- ISAKSEN K., HOLMLUND P., SOLLID J.L. and HARRIS C. 2001. Three Deep Alpine-Permafrost Boreholes in Svalbard, and Scandinavia. *Permafrost and Periglacial Processes* 12: 13–25.
- ISAKSEN K., HAUCK C., GUDEVANG E., ØDEGÅRD R.S. and SOLLID J.L. 2002. Mountain permafrost distribution in Dovrefjell and Jotunheimen, southern Norway, based on BTS and DC resistivity tomography data. *Norsk Geografisk Tidsskrift* 56: 122–136.

- JECKEL P.P. 1988. Permafrost and its altitudinal zonation in N. Lappland. In: Senneset K., (ed.) *Proceedings, Fifth International Conference on Permafrost Vol. 1. Tapir Publishers*, Trondheim: 170–175.
- JOHANSSON M., AKERMAN J., KEUPER F., CHRISTENSEN T.R., LANTUIT H. and CALLAGHAN T.V. 2011. Past and Present Permafrost Temperatures in the Abisko Area: Redrilling of Boreholes. *Ambio* 40: 558–565.
- JONASSON C. 1991. *Holocene slope processes of periglacial mountain areas in Scandinavia and Poland*. Uppsala, Uppsala University Department of Physical Geography UNGI Rapport 79: 156 pp.
- JONSELL U., HOCK R. and DUGUAY M. 2013. Recent air and ground temperature increases at Tarfala Research Station, Sweden. *Polar Research* 32: 1–11.
- KARLÉN W. 1976. Lacustrine sediments and tree-limit variations as indicators of Holocene climatic fluctuations in Lappland, northern Sweden. *Geografiska Annaler* 58 A: 1–33.
- KARLÉN W. 1979. Deglaciation dates from northern Swedish Lappland. *Geografiska Annaler* 61 A: 203–210.
- KASPRZAK M. 2015. High-resolution electrical resistivity tomography applied to patterned ground, Wedel Jarlsberg Land, south-west Spitsbergen. *Polar Research* 34: 25678.
- KING L. 1984. Permafrost in Skandinavien – Untersuchungsergebnisse aus Lappland, Jotunheimen und Dovre/Rondane. *Heidelberger Geographische Arbeiten* 76: 1–125.
- KING L. 1986. Zonation and ecology of high mountain permafrost in Scandinavia. *Geografiska Annaler* 68 A: 131–139.
- KLEMAN J. and GLASSER N.F. 2007. The subglacial thermal organization (STO) of ice sheets. *Quaternary Science Reviews* 26: 585–597.
- KLEMAN J., STROEVEN A.P. and LUNDQVIST J. 2008. Patterns of Quaternary ice sheet erosion and deposition in Fennoscandia and a theoretical framework for explanation. *Geomorphology* 97: 73–90.
- KNEISEL C. 1999. Permafrost in Gletschervorfeldern. Eine vergleichende Untersuchung in den Ostschweizer Alpen und Nordschweden. *Trierer Geographische Studien* 22: 156 pp.
- KNEISEL C. 2003. Permafrost in recently deglaciated glacier forefields – measurements and observations in the eastern Swiss Alps and northern Sweden. *Zeitschrift für Geomorphologie* 47: 289–305.
- KNEISEL C. 2010. The nature and dynamics of frozen ground in alpine and subarctic periglacial environments. *The Holocene* 20: 423–445
- KNEISEL C., and HAUCK C., 2008. Electrical methods. In: Hauck C. and Kneisel C. (eds) *Applied Geophysics in Periglacial Environments*. Cambridge University Press, Cambridge: 3–27.
- KNEISEL C., HAUCK C., FORTIER R. and MOORMAN B. 2008. Advances in geophysical methods for permafrost investigations. *Permafrost and Periglacial Process* 19: 157–178.
- KRAINER K., BRESSAN D., DIETRE B., HAAS J.N., HAJDAS I., LANG K., MAIR V., NICKUS U., REIDL D., THIES D. and TONIDANDEL D. 2015. A 10,300-year-old permafrost core from the active rock glacier Lazaun, southern Ötztal Alps (South Tyrol, northern Italy). *Quaternary Research* 83: 324–335.
- KUKKONEN I.T. and ŠAFANDA J. 2001. Numerical modelling of permafrost in bedrock in northern Fennoscandia during the Holocene. *Global and Planetary Change* 29: 259–273.
- KULLMAN L. and KJÄLLGREN L. 2006. Holocene pine tree-line evolution in the Swedish Scandes: Recent tree-line rise and climate change in a long-term perspective. *Boreas* 35: 159–168.
- LILLEØREN K.S., ETZELMÜLLER B., SCHULER T.V., GISNÅS K. and HUMLUM O. 2012. The relative age of mountain permafrost — estimation of Holocene permafrost limits in Norway. *Global and Planetary Change* 92–93: 209–222.

- LOKE M.H., CHAMBERS J.E., RUCKER D.F., KURAS O. and WILKINSON P.B. 2013. Recent developments in the direct current geoelectrical imaging method. *Journal of Applied Geophysics* 95: 135–156.
- LOKE M.H. 2014. *Tutorial: 2-D and 3-D electrical imaging; surveys*: <http://www.geoelectrical.com> (Website accessed 26.04.2014).
- MARESCOT L., LOKE M.H., CHAPPELLIER D., DELALOYE R., LAMBIEL C. and REYNARD E. 2003. Assessing reliability of 2D resistivity imaging in mountain permafrost studies using the depth of investigation index method, *Near Surface Geophysics* 1: 57–67.
- MARKLUND P. 2011. *Alpin permafrost I Kebnekaiseffjällen: Modellering med logistic regression och BTS-data. Självständigt arbete i geovetenskap*. Nr. 22, Uppsala University, Disciplinary Domain of Science and Technology, Earth Sciences, Department of Earth Sciences, LUVAL. Uppsala: 29 pp. [in Swedish].
- MELANDER O. 1977. *Geomorfologiska kartbladet 30 J. Rensjön*. SNV PM 858.
- OLDENBURG D.W. and LI Y. 1999. Estimating depth of investigation in dc resistivity and IP surveys, *Geophysics* 64: 403–416.
- OLDENBURG D.W. and JONES F.H.M. 2007. *Inversion for Applied Geophysics; Learning resources about geophysical inversion*, University of British Columbia: Geophysical Inversion Facility, <http://www.eos.ubc.ca/ubcgif/iag/index.htm> (Website accessed 26.04.2014).
- ØDEGÅRD R.S., HOELZLE M., JOHANSEN K.V., and SOLLID J.L. 1996. Permafrost mapping and prospecting in southern Norway. *Norsk Geografisk Tidsskrift* 50: 41–54.
- ØSTREM G. 1964. Ice-cored moraines in Scandinavia. *Geografiska Annaler* 46: 282–337.
- RAPP A. 1982. Zonation of permafrost indicators in Swedish Lapland. *Geografisk Tidsskrift* 82: 37–38.
- REYNOLDS J.M. 2011. *Electrical resistivity methods. An Introduction to Applied and Environmental Geophysics*. Wiley, Chichester: 289–372.
- RIDEFELT H., ETZELMÜLLER B., BOELHOUWERS J. and JONASSON C. 2008. Statistic-empirical modelling of mountain permafrost distribution in the Abisko region, sub-Arctic northern Sweden. *Norsk Geografisk Tidsskrift Norwegian Journal of Geography* 62: 278–289.
- SAWADA Y., ISHIKAWA M. and ONO Y. 2003. Thermal regime of sporadic permafrost in a block slope on Mt. Nishi-Nupukaashinupuri, Hokkaido Island, Northern Japan. *Geomorphology* 52: 121–130.
- SCAPOZZA C., LAMBIEL C., BARON L., MARESCOT L. and REYNARD E. 2011. Internal structure and permafrost distribution in two alpine periglacial talus slopes, Valais, Swiss Alps. *Geomorphology* 132: 208–221.
- SCHMIDT P., LUND B., NÅLSUND J.-O. and FASTOK J. 2014. Comparing a thermo-mechanical Weichselian Ice Sheet reconstruction to reconstructions based on the sea level equation: aspects of ice configurations and glacial isostatic adjustment. *Solid Earth* 5: 371–388.
- SCHROTT L. and SASS S. 2008. Application of field geophysics in geomorphology: advances and limitations exemplified by case studies. *Geomorphology* 93: 55–73.
- SEPPÄLÄ M. 1982. Present-day periglacial phenomena in northern Finland. *Biuletyn Peryglacjalny* 29: 231–243.
- SIEGERT M.J., DOWDESWELL J.A., HALD M. and SVENDSEN J.-I. 2001. Modelling the Eurasian Ice Sheet through a full (Weichselian) glacial cycle. *Global and Planetary Change* 31: 367–385.
- SZEWczyk J. 2017. The deep-seated low land relict permafrost from the Suwałki region (NE Poland) – analysis of conditions of its development and preservation. *Geological Quarterly* 61: 845–858.
- SZEWczyk J. and NAWROCKI J. 2011. Deep-seated relict permafrost in northeastern Poland. *Boreas* 40: 385–388.

- ŠAFANDA J., SZEWCZYK J. and MAJOROWICZ J. 2004. Geothermal evidence of very low glacial temperatures on a rim of the Fennoscandian ice sheet. *Geophysical Research Letters* 31: L07211.
- WINKLER S., MATTHEWS J.A., MOURNE R.W. and WILSON P. 2016. Schmidt-hammer exposure ages from periglacial patterned ground (sorted circles) in Jotunheimen, Norway, and their interpretative problems. *Geografiska Annaler* 98A: 265–285.
- YERSHOV E.D. 1992. *Kriolitogenez.* Nerda, Moskva: 211 pp. [in Russian].
- YOSHIKAWA K., LEUSCHEN C., IKEDA A., HARADA K., GOGINENI P., HOEKSTRA P., HINZMAN L., SAWADA Y. and MATSUOKA N. 2006. Comparison of geophysical investigations for detection of massive ground ice (pingo ice). *Journal of Geophysical Research* 111: E06S19.
- YOU Y., YU Q., PAN X., WANG X. and GUO L. 2013. Application of electrical resistivity tomography in investigating depth of permafrost base and permafrost structure in Tibetan Plateau. *Cold Regions Science and Technology* 87: 19–26.

Received 7 July 2017

Accepted 13 April 2018